

Exciton polaritons in thin films

R. N. Philp* and D. R. Tilley

Department of Physics, University of Essex, Colchester CO4 3SQ, England

(Received 20 June 1990; revised manuscript received 17 May 1991)

When excitons are coupled to light in the band-gap frequency region, they form exciton polaritons. Dispersion relations are calculated for *s*- and *p*-polarized exciton polaritons in thin films. The film is assumed to be isotropic, with a response function governed by a single excitonic resonance. Solutions are generated and interpreted in terms of limiting cases for an idealized material. The solutions are investigated for two additional boundary conditions $\mathbf{u}=\mathbf{0}$ and $\hat{\mathbf{n}}\cdot\nabla\mathbf{u}=\mathbf{0}$, where $\hat{\mathbf{n}}$ is a vector normal to the boundary and \mathbf{u} is the excitonic field, and numerical results are presented for a free-standing film. The method of attenuated total reflection (ATR) is suggested as a means of detecting thin-film exciton polaritons. A semiclassical approach is presented to calculate the reflection coefficient in such an experiment. Both *s* (TE) and *p* (TM) polarizations are considered. We also generate the associated dispersion curves for an asymmetric geometry so that a comparison can be made between the two sets of calculations. The film is assumed thick enough to have isotropic bulk properties and attention is restricted to a single excitonic resonance. We apply the theory to a film of GaAs on a substrate of NaF, with a vacuum on the other side of the film. The prism in the ATR calculations is assumed to be ZnS. The additional boundary condition required for the problem is taken to be $M\mathbf{u}+N\partial\mathbf{u}/\partial z=\mathbf{0}$, where \mathbf{u} is the excitonic field and the normal to the interfaces is in the *z* direction. The theoretical results are presented in the full form of the additional boundary condition but we investigate numerically the extremes $\mathbf{u}=\mathbf{0}$ and $\partial\mathbf{u}/\partial z=\mathbf{0}$.

I. INTRODUCTION

The coupling of light to excitons in semiconductors has been the subject of intensive study for many years. Pekar,^{1,2} Hopfield,³ and Hopfield and Thomas^{4,5} dealt with the polariton modes formed by exciton-photon coupling in a bulk material, and in particular showed that spatial dispersion leads to significantly different behavior from the simpler case of phonon polaritons. Later, Maradudin and Mills⁶ developed a theory of surface exciton polaritons and demonstrated that due to spatial dispersion the surface mode is leaky, with energy loss into the continuum of bulk exciton polaritons of the same frequency. In this paper we deal with exciton polaritons (EP's) in a film of finite thickness. We use a macroscopic form of the additional boundary condition (ABC), and for this reason the results are strictly applicable only for $a \gg a_B$, where a is the film thickness and a_B is the excitonic Bohr radius, typically of the order 10 nm.

Although the results are designed in the first instance for films, it is hoped that they will give some preliminary insight into EP formation in quantum wells (QW's). Due to the confinement of electronic wave functions, excitons in QW systems have markedly different characteristics from those in bulk semiconductors. The experiments of Dingle⁷ and the theoretical results of Greene, Bajaj, and Phelps,⁸ on the behavior of excitons in GaAs/Al_xGa_{1-x}As layered materials both indicate that bulk excitonic properties, e.g., binding energies and oscillator strengths, remain relatively unaltered for layers of GaAs down to widths of $a \approx 5a_B$, where a_B is the Bohr radius in GaAs. Absorption spectra for multiple-

quantum-well (MQW) systems below this limit show higher principal resonances together with their associated light-hole and heavy-hole resonances. These appear with increasing resolution for decreasing well width. In addition, well-width reduction produces an increase in energy at which resonant absorption occurs. This process reaches a maximum when $a \approx a_B$; below this point the absorption peaks shift back down the energy scale, tending to the absorption spectra for Al_xGa_{1-x}As, the material of the cladding layers. Since our calculations in any case assume $a \gg a_B$, we believe them to be applicable to wide QW's.

EP's exhibit the effects of spatial dispersion, that is, a wave-number dependence of the dielectric function. The simplest relevant form of the dielectric function is

$$\epsilon(k, \omega) = \epsilon_\infty + S / (\omega_e^2 + Dk^2 - \omega^2 - i\omega\Gamma). \quad (1)$$

Here ϵ_∞ is the background dielectric constant and S is the dipole strength of the exciton, ω_e is the band-gap frequency less the binding frequency, and $D = \hbar\omega_e/M$, where $M = m_e + m_h$ is the exciton mass. Finally, Γ is a phenomenological damping parameter, which will mainly be neglected in what follows. Equation (1) differs from the corresponding phonon form by the spatial-dispersion term Dk^2 .

The bulk EP dispersion relation is found by solving Maxwell's equations with the use of the dielectric function (1). The result is

$$\epsilon(k, \omega)[k^2 - \epsilon(k, \omega)\omega^2/c^2] = 0. \quad (2)$$

This gives a longitudinal mode if $\epsilon(k, \omega) = 0$ and a transverse mode if the second factor vanishes. The dispersion

curve for the transverse mode, which together with the longitudinal is shown in Fig. 1, resembles that for the phonon polariton, except that the lower branch bends up for large k . This is due to spatial dispersion, and the asymptotic form of the lower branch is $\omega^2 \approx \omega_e^2 + Dk^2$. The most important qualitative change is that there is no stop band in the dispersion curve; there is at least one propagating mode for every frequency ω . A useful way to look at (2) and Fig. 1 is that for a given ω there are three roots k_j : one real and two imaginary for $\omega < \omega_L$, and three real for $\omega > \omega_L$.

Figure 1 brings out a major point of interest. Suppose s -polarized light is incident from vacuum on the surface of an excitonic medium. Two transverse modes of wave numbers k_1 and k_2 , say, can propagate in the medium. It should therefore be possible to evaluate two transmission coefficients T_1 and T_2 as well as a reflection coefficient R . However, Maxwell's equations provide only two boundary conditions, so an ABC is required. The need for an ABC was first recognized by Pekar,¹ and has been a recurrent problem since then. Helpful discussions and references are given by Maradudin and Mills,⁶ So *et al.*,^{9,10} Halevi,¹¹⁻¹³ Nkoma,¹⁴ Matsushita, Wickstead, and Cummins,¹⁵ Del Sole and D'Andrea,¹⁶ and Basilev,¹⁷ among others. The most frequently adopted view, as summarized by Halevi,¹² is that just below the surface, at $z=0$ say, there is an exciton-free, or dead, layer of thickness a_D in which the exciton polarization \mathbf{P}_e is zero. On the other side of the dead layer at $z=-a_D$, \mathbf{P}_e satisfies an ABC most often taken as $\mathbf{P}_e=0$ (e.g., Pekar,¹ Hopfield and Thomas^{4,5}) or $\partial\mathbf{P}_e/\partial z=0$ (e.g., Ting *et al.*¹⁸). The most recent use of the ABC $\mathbf{P}_e=0$ is by Ivchenko and Kosobukin,¹⁹ who use it to calculate the dispersion relation for an infinite superlattice. Halevi,¹² following Agarwal, Pattanayk, and Wolf²⁰ and others, made use of the parametrized combination

$$\mathbf{P}_e + \xi \partial \mathbf{P}_e / \partial z = 0, \quad (3)$$

which obviously includes $\mathbf{P}_e=0$ and $\partial\mathbf{P}_e/\partial z=0$ as special cases. Del Sole and D'Andrea¹⁶ employ a microscopic model to refine the dead-layer picture. In their model, there is a transition layer of between $0.5a_B$ and a_B at the surface, where a_B is the effective Bohr radius within the semiconductor, typically of the order 10 nm. Within the transition layer the behavior of \mathbf{P}_e is complicated, but the behavior of \mathbf{P}_e as $z \rightarrow 0.5a_D$ is described by the ABC(3). The relation between their approach and the coherent wave model of Basilev¹⁷ is discussed by Del Sole and D'Andrea.¹⁶ This picture, of complicated microscopic behavior within a transition layer leading to a relatively simple macroscopic ABC of the form (3), is similar to what is found for the proximity effect in superconductivity (de Gennes²¹).

For p -polarized incident light the situation is somewhat more complicated. In addition to the two transverse modes, a longitudinal mode is excited. The ABC (3) now has two components, so that altogether there are four boundary conditions. The number of boundary conditions is now sufficient to determine the reflection coefficient R , two "transverse" transmission coefficients T_1 and T_2 , and a "longitudinal" transmission coefficient T_L . Expressions for the reflection and transmission coefficient in both s and p polarization with the ABC (3) are given by Tilley²² and Nkoma.¹⁴

The use of a differential formulation of Maxwell's equations together with standard boundary conditions and an ABC is the commonest way of treating exciton-photon coupling. Alternatively, the constitutive relation between \mathbf{D} and \mathbf{E} , or between \mathbf{P} and \mathbf{E} , can be written as an integral equation. In this case the integral kernel $\epsilon(\mathbf{r}-\mathbf{r}',\omega)$ is effectively the Fourier transform of $\epsilon(k,\omega)$, but the ABC is already included within the integral formulation. The equivalence of an integral formulation to a differential equation together with an ABC is demonstrated explicitly elsewhere²² for some simple examples.

The theory of the surface EP was first given by Maradudin and Mills.⁶ An important qualitative difference between this case and the surface phonon polariton is that there is no stop band in the bulk dispersion curve. Even in the interval $\omega_e < \omega < \omega_L$ a bulk mode exists, as seen in Fig. 1; its origin is clearly in the spatial dispersion term Dk^2 of (1). This means that although something like a surface mode exists in $\omega_e < \omega < \omega_L$, even in the absence of damping [$\Gamma=0$ in (1)], the dispersion relation does not have solutions with real ω and k_x . For real ω , k_x is complex: if a mode is launched along the surface, it decays with an attenuation length $2\pi/\text{Im}(k_x)$. Physically the field energy of the mode is transferred to bulk modes of the same frequency, so that the surface EP is leaky.

In the present work we extend the study of Maradudin and Mills⁶ to a film of thickness a . In a film, the bulk-mode continuum is replaced by the guided-wave spectrum. The energy transfer then leads to mode mixing between the surface and guided modes, so that in the absence of damping we expect to find undamped normal modes that have mixed surface and guided character. In this sense, the film presents a simpler problem, at least

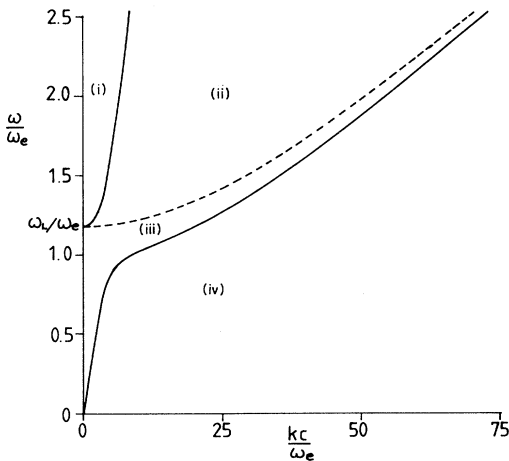


FIG. 1. Schematic bulk exciton-polariton curves. —, transverse modes; - - - longitudinal mode. Regions (i)-(iv) correspond to different signs of the quantities K_1^2 , K_2^2 , and K_L^2 defined subsequently: (i) $K_1^2 < 0$, $K_2^2 < 0$, $K_L^2 < 0$; (ii) $K_1^2 < 0$, $K_2^2 > 0$, $K_L^2 < 0$; (iii) $K_1^2 < 0$, $K_2^2 < 0$, $K_L^2 > 0$; (iv) $K_1^2 > 0$, $K_2^2 > 0$, $K_L^2 > 0$.

conceptually, than the semi-infinite medium. The results apply directly to a thin film of an excitonic medium such as GaAs or Cu_2O , say, which have been used in experimental studies of the kind mentioned above. In addition, it is hoped that they contain the essential physics of EP propagation in QW systems. In a QW, GaAs in $\text{Al}_x\text{Ga}_{1-x}\text{As}$ say, the well is contained within a cladding material which has a larger band gap. The more rigorous discussions of ABC's, such as that by Del Sole and D'Andrea,¹⁶ deal with a free surface rather than an interface with another semiconductor. However, it is likely that a model based on transition layer together with ABC (3) will continue to apply, so that our results should be relevant for QW's of thickness $a \gg a_B$. In fact, experimental results on reflectivity and photoluminescence by Tuffigo *et al.*²³ and by Schultheis and Ploog²⁴ show clear structure due to confined EP's of the kind to be described. Similarly, the reflectance experiments on thin-film CdSe by Kiselev *et al.*, Razbirin, and Ural'tsev²⁵ show clear structure.

It is convenient to reformulate (1) and (3) by introducing an excitonic field \mathbf{u} , following Tilley.²² The field equation for \mathbf{u} is taken as

$$\ddot{\mathbf{u}} + \Gamma \dot{\mathbf{u}} = D \nabla^2 \mathbf{u} - \omega_c^2 \mathbf{u} + (\epsilon_0 S)^{1/2} \mathbf{E}, \quad (4)$$

where E is the macroscopic electric field. The macroscopic polarization \mathbf{P} is related to \mathbf{u} and \mathbf{E} by means of

$$\mathbf{P} = (\epsilon_0 S)^{1/2} \mathbf{u} + \epsilon_0 (\epsilon_\infty - 1) \mathbf{E} \quad (5)$$

in which the first term on the right-hand side is the excitonic polarization \mathbf{P}_e . Elimination of \mathbf{u} between (4) and (5), together with the use of the definition $\epsilon_0 \mathbf{E} + \mathbf{P} = \epsilon_0 \epsilon \mathbf{E}$, gives the dielectric function (1). Equations (4) and (5) are the extension to the excitonic medium of the well-known Born-Huang²⁶ treatment of dielectric properties in the reststrahl frequency region. As the boundaries of the film we apply the dead-layer, or transition-layer, model with ABC (3). As discussed above, the dead layer has thickness $a_D \leq a_B$, and therefore $a_D \ll a$. The dead layer is an exciton-free region, so from the electromagnetic point of view it behaves as a thin cladding of an ordinary dielectric. Since $\lambda \gg a_D$, λ being the free space wavelength (typically $a_D \approx 5$ nm and $\lambda \approx 700$ nm), the dead layer has negligible effect on the polariton properties to be discussed. Inclusion of the dead layer would greatly complicate the algebra without affecting the results significantly; we therefore omit it and apply the ABC (3) at the boundary surfaces $z = \pm a/2$. The boundary condition (3) is taken in the equivalent form

$$M\mathbf{u} + L \partial \mathbf{u} / \partial z = 0 \quad (6)$$

and for simplicity we restrict attention in numerical work to the extreme cases $M = 1, L = 0$ and $M = 0, L = 1$.

It is worth clarifying the relationship between our model and that proposed by Schultheis and Ploog²⁴ in connection with their results on the reflectivity of single and double QW's. They employed thin wells, $a \approx a_B$, and therefore postulated a dielectric function of the form (1), but with k as the in-plane wave vector. This is appropriate, since the motion transverse to the well is quantized in

a thin well, and so there is no transverse wave-vector component. Consequently, there is no spatial dispersion transverse to the well, and hence no need for an ABC. As already emphasized, we are considering the opposite limit $a \gg a_B$.

There have been many experimental studies of bulk exciton polaritons, including reflection, transmission, and fluorescence spectroscopy (Knox,²⁷ Kuper and Whitfield²⁸); resonance Raman scattering (Washington *et al.*²⁹); and perhaps most successfully resonant Brillouin scattering, first proposed by Brenig, Zeyher, and Birman³⁰ and subsequently investigated by Weisbuch and Ulbrich,³¹ Hermann and Yu,³² Sermage and Fishman,³³ Tilley,²² and So *et al.*,^{9,10} among others.

The major technique for study of electromagnetically couple surface excitations is attenuated total reflection (ATR), first applied in this way by Otto.³⁴ The early applications of ATR were to surface phonon and plasmon polaritons, in which the effects of spatial dispersion are usually unimportant. The technique was later applied to surface exciton polaritons in a number of materials: CuBr (Lagois and Fischer³⁵), ZnO (Lagois and Fischer³⁶), CuBr (Hirabayashi, Tokura, and Koda³⁷), and ZnSe (Tokuru, Hirabayashi and Koda³⁸). Much of the theoretical work for semi-infinite spatially dispersive materials has been carried out by Maradudin and Mills,⁶ Rimbey,³⁹ and Lagois and Fischer.⁴⁰

Thin films of spatially dispersive materials have been observed with normal-incidence reflection/transmission measurements on CdS and CdSe crystals (Kiselev *et al.*^{25,41,42}); reflectance experiments on GaAs/ $\text{Al}_x\text{Ga}_{1-x}\text{As}$ quantum-well structures (Zheng *et al.*⁴³); reflectance, excitation, and luminescence spectra of GaAs/ $\text{Al}_x\text{Ga}_{1-x}\text{As}$ quantum wells (Schultheis and Ploog,²⁴); and photoluminescence spectra of thin-layer heterostructures of the type $\text{Cd}_{1-x}\text{Zn}_x\text{Te}/\text{CdTe}/\text{Cd}_{1-x}\text{Zn}_x\text{Te}$ (Tuffigo *et al.*²³). Yang, Sambles, and Bradberry⁴⁴ have applied ATR to prove the existence of a long-range coupled surface exciton polariton in a thin vanadium film. However, they describe the mode under study as an exciton polariton because the strong resonance from which it arises is of interband character, and they do not find it necessary to include spatial dispersion. Similarly, Kohl *et al.*^{4,5} analyze their results on photoluminescence from grating-coupled exciton polaritons in MQW structures without the inclusion of spatial dispersion.

Of particular relevance to this paper is the photoluminescence study on GaAs thin films carried out by Kusano *et al.*⁴⁶ They deal with films of thickness 99 and 201 nm, which are thick enough for the excitons to be of three-dimensional (3D) character but which are at the same time thin enough for quantization of the exciton transverse motion to lead to discrete photoluminescence peaks. This is the range of thickness that we are considering. Kusano *et al.* estimate values of k (effectively k_z) from a simple quantization argument in which a dead layer is included at each surface. The (ω, k) values for the ten or so photoluminescence peaks they observe fit very well to the known bulk exciton-polariton dispersion curve³¹ for the thicker film, but for the thinner film there

is a systematic discrepancy, perhaps due to the influence of film thickness on the excitonic parameters. The model invoked by Kusano *et al.* is exactly the one that is analyzed in detail here.

In view of the importance of the ATR technique, we have calculated ATR spectra corresponding to our theoretical thin-film exciton-polariton dispersion curves; the results are illustrated for a GaAs film on a NaF substrate.

The plan of the paper is as follows. In Secs. II and III we calculate dispersion curves for *s*- and *p*-polarized modes, respectively. In order to present the results simply as graphs of real frequency versus real wave vector we omit damping in these sections. The corresponding ATR spectra are derived and illustrated in Sec. IV. Conclusions are presented in Sec. V.

II. DISPERSION CURVES: *s* POLARIZATION

We take an excitonic film characterized by (1) in $-a/2 < z < a/2$ with isotropic media having dielectric constants ϵ_1 and ϵ_3 occupying the regions $z > a/2$ and $z < -a/2$. The *x* axis is taken as the propagation direction, so that the electromagnetic fields in all three media have the common factor $\exp(ik_x x - i\omega t)$. In *s* polarization the electric fields are in the *y* direction, and we write them in the form

$$E_y = \begin{cases} E_1 \exp[-\kappa_1(z - a/2)], & z > a/2 \\ \sum_{j=1,2} [E_{1j} \exp(K_j z) + E_{2j} \exp(-K_j z)], & -\frac{a}{2} \leq z \leq \frac{a}{2} \\ E_3 \exp[\kappa_3(z + a/2)], & z < -a/2. \end{cases} \quad (7a)$$

$$-\frac{a}{2} \leq z \leq \frac{a}{2} \quad (7b)$$

$$E_3 \exp[\kappa_3(z + a/2)], \quad z < -a/2. \quad (7c)$$

Here κ_1 and κ_3 are given by

$$\kappa_i^2 = k_x^2 - \epsilon_i \omega^2 / c^2 \quad (8)$$

and both must be real in order that the mode be localized on the film. The two constants K_1 and K_2 are given by the condition that the second factor of (2) vanish with \mathbf{k} in the form $(k_x, 0, iK_j)$; it is seen from (1) that this equation is a quadratic in K_j^2 , so that it does indeed have two roots.

The dispersion equation for the modes is found by applying the standard electromagnetic boundary conditions together with the ABC (6) to the fields in (7). This produces a 6×6 determinant since there are six field amplitudes in (7), but this determinant can be written in a somewhat simpler form. The general result is given elsewhere,⁴⁷ the result for the simpler case of a symmetric geometry $\epsilon_1 = \epsilon_3$ is given in Appendix A.

An example of the dispersion curves for the symmetric geometry is shown in Fig. 2. In discussing these curves it is helpful to refer to the regions (i) to (iv) marked in Fig. 1, which as the caption makes clear correspond to various combinations of surface-type (K real) and guided type (K imaginary) behavior within the film. The values chosen here for D and ω_L are deliberately large so as to

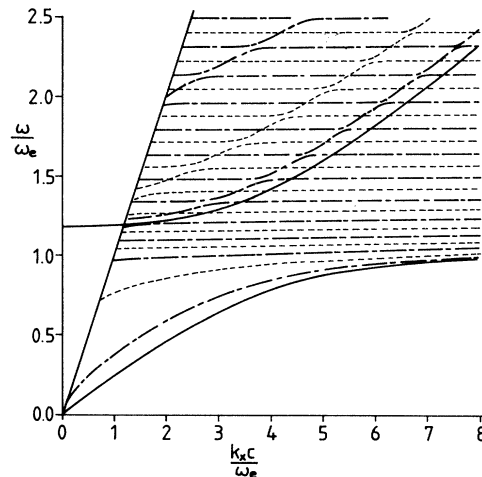


FIG. 2. *s*-polarized thin-film exciton-polariton dispersion curves for ABC $\mathbf{u}=\mathbf{0}$. The dielectric function parameters are $\epsilon_1=1$, $\epsilon_\infty=10$, $D=10^{-3}c^2$, $\omega_L/\omega_e=1.18$, and the film thickness is $a=c/\omega_e$. -----, even modes; , odd modes.

bring out important qualitative points. For the ABC $\mathbf{u}=\mathbf{0}$ ($L=0$) used in Fig. 2, (A1) reduces to a product of two determinants corresponding to modes of even and odd symmetry as indicated in Fig. 2. The parts of the dispersion curves lying in regions (i) and (iii) are essentially excitonlike: they correspond closely to solutions of (4) with $S=0$ and the ABC applied at the film surfaces. They are standing-wave excitons within the film, and coupling to the electromagnetic field is of little importance. In the guided-wave region (i), however, each dispersion curve passes through excitonlike and polaritonlike parts. The curves in this region have the character of standing excitons superposed on guided-wave (standing) polaritons, with crossings between modes of the same symmetry removed by the coupling.

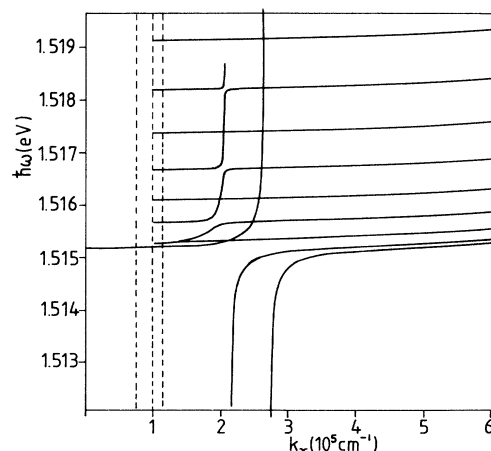


FIG. 3. *s*-polarized thin-film exciton-polariton dispersion curves for a 0.1- μm GaAs film on a NaF substrate with ABC $\mathbf{u}=\mathbf{0}$.

The more practical case for experiments is the nonsymmetric geometry $\epsilon_1 \neq \epsilon_3$. For calculations in this case we take realistic parameters for a GaAs film on a NaF substrate. The dielectric constant of NaF (Ref. 48) is 1.756, and the parameters for GaAs are⁴⁹ $\omega_e = 1.5151$ eV $\Gamma = 0.035$ meV, $\epsilon_\infty = 12.65$, $D/c^2 = 4.9 \times 10^{-6}$, and $S/\omega_e^2 = 0.133 \times 10^{-2}$. For calculation of dispersion curves Γ is set equal to zero, but the actual value is needed later for ATR calculations.

A set of dispersion curves for the ABC $\mathbf{u} = 0$ is shown in Fig. 3. Although the geometry is asymmetric the modes do still divide approximately into evenlike and oddlike, and it is seen that as in Fig. 2 crossings are removed between modes of the same symmetry. Since we shall subsequently discuss ATR spectra, Fig. 3 includes, as the right-hand member of the three nearly vertical dashed lines, the ATR scan line $k_x = \epsilon_p^{1/2}(\omega/c)\sin\theta$ for a ZnS prism ($\epsilon_p = 5.616$) and angle of incidence $\theta = 40.1^\circ$. Also shown are the vacuum and substrate light lines $k_x = \omega/c$ and $\epsilon_3^{1/2}\omega/c$.

We have also calculated⁴⁷ dispersion curves for the ABC $\partial u / \partial z = 0$. These have a generally similar character to those shown in Figs. 2 and 3, but the mode anticrossing gaps are much less pronounced.

III. DISPERSION CURVES: *p* POLARIZATION

In this case the E field is the x - z plane and takes the form

$$\mathbf{E} = \begin{cases} (1, 0, ik_x/\kappa_1)E_1 \exp[-\kappa_1(z-a/2)], & z < a/2 & (9a) \\ \mathbf{E}_1 + \mathbf{E}_2 + \mathbf{E}_L, & -a/2 < z < a/2 & (9b) \\ (1, 0, -ik_x/\kappa_3)E_3 \exp[\kappa_3(z+a/2)], & z < -a/2. & (9c) \end{cases}$$

Here the component transverse and longitudinal fields in the film are

$$\mathbf{E}_j = (1, 0, ik_x/K_j)E_{1j} \exp(-K_j z) + (-1, 0, ik_x/K_j)E_{2j} \exp(K_j z), \quad j = 1, 2 \quad (10)$$

$$\mathbf{E}_L = (1, 0, K_L/ik_x)E_{1L} \exp(K_L z) + (1, 0, -K_L/ik_x)E_{2L} \exp(-K_L z). \quad (11)$$

K_1 and K_2 were defined previously, under (8); K_L is defined by the equation $\epsilon(k, \omega) = 0$ with $\mathbf{k} = (k_x, 0, iK_L)$.

The dispersion equation is now an 8×8 determinant rather than 6×6 since the two longitudinal amplitudes E_{1L} and E_{2L} are included. For the symmetric geometry $\epsilon_1 = \epsilon_3$ it reduces to the 6×6 determinant given in Appendix A; the result for the general case is given in Ref. 47.

The inclusion of the longitudinal component means that in the absence of coupling to the electromagnetic field there are twice as many standing-exciton modes as for s polarization. The polariton curves, with coupling included, are therefore more complicated, so we show the even- and odd-parity modes for ABC $\mathbf{u} = 0$ separately, in Figs. 4 and 5, respectively. In the predominantly exciton region (ii) the modes are alternately transverse and longitudinal. As for s polarization, in region (i) the dispersion

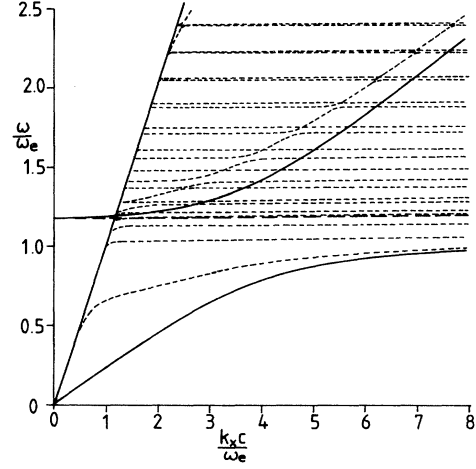


FIG. 4. p -polarized thin-film exciton-polariton dispersion curves for ABC $\mathbf{u} = 0$ even modes. The parameters are film thickness $a = c/\omega_e$, $\omega_L/\omega_e = 1.18$, $D = 10^{-3}c^2$.

curves may be seen as resulting from mixing of excitonlike and polaritonlike modes. As might be expected, the polariton-transverse-exciton mixing is considerably stronger than the polariton-longitudinal-exciton mixing. In the pure phonon-polariton case, with no spatial dispersion, a distinguishing feature of p polarization is the occurrence of an even and an odd surface mode within the bulk stop band $\omega_T < \omega < \omega_L$. The analog of these modes can be discerned in Figs. 4 and 5.

For the asymmetric case, dispersion curves for GaAs film on a NaF substrate are shown in Fig. 6 with the same parameters as used for Fig. 3. Comparison with Fig. 3 shows the additional structure due to the inclusion of the longitudinal component in the film.

For p polarization as for s polarization, the dispersion

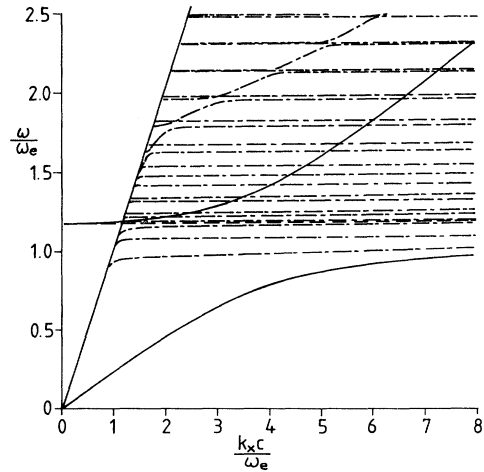


FIG. 5. p -polarized thin-film exciton-polariton dispersion curves for ABC $\mathbf{u} = 0$ odd modes. The same parameters and notation as in Fig. 4.

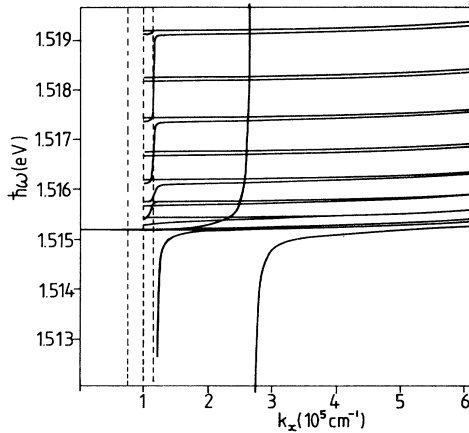


FIG. 6. p -polarized thin-film exciton-polariton dispersion curves for a $0.1\text{-}\mu\text{m}$ GaAs film on a NaF substrate with ABC $\mathbf{u}=\mathbf{0}$. As in Fig. 3, the two light lines $k_x = \omega/c$, $k_x = \epsilon_3^{1/2}\omega/c$ and an ATR scan line $k_x = \epsilon_p^{1/2}(\omega/c)\sin\theta$ are shown as the three near-vertical dashed lines.

curves for ABC $\partial\mathbf{u}/\partial z = \mathbf{0}$ are similar in general character, but the mode repulsions are much less pronounced.⁴⁷

IV. ATR SPECTRA

We now proceed to the second main calculation of this paper, the ATR spectrum of thin-film exciton polaritons. For a general discussion of ATR we refer to Cottam and Tilley⁵⁰ and Abeles.⁵¹ We present calculations for the Otto configuration shown in Fig. 7. Fukui, Kamada, and Toda⁵² calculated the ATR spectrum for a film of ZnO, which has a wurtzite structure, but there the anisotropy of the crystal structure reduced the number of fields required in the analysis, and in addition they assumed the prism to be in contact with the film. In the following calculation we retain all the fields and include a gap between the prism and the film so that the postulated experiment

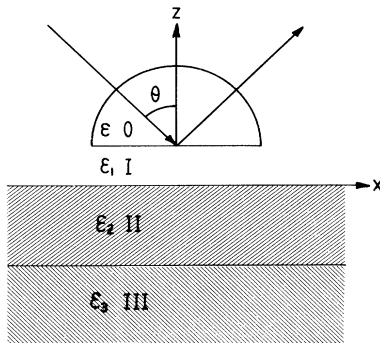


FIG. 7. The prism and thin-film configuration used in the ATR calculations. We take the prism to be ZnS, and the prism-film separation as 0.1 and $0.25\ \mu\text{m}$ for s and p polarization, respectively; all other parameters are those indicated in the text. The scan line employed in the subsequent spectra is the right-most finely dashed line of Figs. 3 and 6.

probes more accurately the modes of the thin film.

Generally, when light enters a prism and undergoes internal reflection an evanescent radiation field is produced at the base of the prism. If the prism is then brought into proximity with a system, such as a thin film, then they become coupled and energy can be transferred from the prism to the system.

We consider the specific system shown in Fig. 7. Media 0, I, and III are assumed isotropic with dielectric constants ϵ , ϵ_1 , and ϵ_3 all of which are independent of frequency and wave number. As before, we assume the film, medium II, to be isotropic with one excitonic resonance. We further assume that the interface at $z=d$ is illuminated from medium 0 with plane polarized light of frequency ω and wave number k in the x - z plane and at an angle θ to the plane normal. The in-plane component of the wave vector is thus $k_x = k \sin\theta$.

The principle of ATR assumes $\epsilon > \epsilon_1$ so that when $\theta > \theta_c = \sin^{-1}(\epsilon_1^{1/2}/\epsilon^{1/2})$, an evanescent electromagnetic field is generated in medium I and couples the prism to the film. When the frequency ω and in-plane wave number k_x of the incident light coincides with a mode of the film, then an excitation is launched along it. This diverts energy away from the reflected beam and into the film, producing a depression in the reflectivity. The diverted energy can then either remain in the film until it is dissipated by damping, if there is an evanescent field in medium III; or it can be diverted into a traveling wave in medium III. The form of the field in medium III depends on where the ATR scan line lies in the k_x - ω plane relative to the light line of the lower cladding medium. In this paper we chose the scan line such that an evanescent field is produced in medium III, since in the generation of Figs. 3 and 6 we assumed exponentially decaying fields in the cladding materials. The shape and sharpness of the depressions in the ATR spectra are largely controlled by the distance between the prism and the specimen, the angle of the incident light to the plane normal θ and by the excitonic damping parameter. The prism must not be too close to the film to produce overcoupling, but also it must not be too far away from the film to produce undercoupling. The angle θ is then chosen to highlight the features of the ATR spectrum.

The method of ATR has been applied to many systems, particularly to the detection of surface modes on semi-infinite media. With a spatially nondispersive medium what generally happens is that the incident light can couple to either a surface mode or one of the infinite bulk modes. This produces either a decaying field or a traveling wave in the semi-infinite medium, but for spatially nondispersive materials, these generally occur in separate frequency ranges. However, the characteristic effect of spatial dispersiveness of the excitons is to overlap the bulk energy bands and so remove the stop band within which the surface excitations usually lie. The overlap of the bands now allows bulk excitations for all frequencies including the frequency range of the surface excitation. Thus any excitation launched along the surface of the semi-infinite medium is coupled to the bulk modes and so leaks away from the surface into the bulk. Mathematically this is represented by one of the complementary

pair ω and k_x of the surface excitation having to be complex even in the absence of damping. This forces the surface excitation to have a decay length or decay time, thus these modes are known as leaky modes. This point is discussed elsewhere, see for instance Maradudin and Mills⁶ or Lagois and Fischer.³⁵ In our present discussion, however, the film is finite, disallowing leaky modes and hence leaving damping as the only mechanism by which energy can be dissipated.

The fields in the ATR calculations are essentially the same as in the corresponding thin-film dispersion calculation. We must, however, extend the field of medium I, Fig. 7, to a superposed evanescent mode and include the incident and reflected plane-polarized light in medium 0. The film is now taken to occupy the space $-a < z < 0$. We take the parameters to be those of Sec. I, in addition we take the prism to be ZnS with a dielectric constant $\epsilon = 5.616$ and the thickness of the gap to be $d = 0.1$ and $0.25 \mu\text{m}$ for s and p polarizations, respectively. In the numerical calculations we fixed the angle θ of the incident light to be $\theta = 40.1^\circ$ and scanned the frequency. The scan line employed in the generation of our results is shown with the dispersion curves of Figs. 3 and 6 as the far right finely dashed line. We also show with the ATR results the relevant portion of the dispersion curves for comparison. As before, we generated the results for the ABC's $\mathbf{u} = \mathbf{0}$ and $\partial \mathbf{u} / \partial z = \mathbf{0}$, but only the former are shown here.

In s polarization there are only two transverse excitations in medium II, $-a < z < 0$ (Fig. 7). We therefore take the electric fields as

$$\mathbf{E}_0 = [0, E_i \exp[-ik_z z] + E_r \exp(ik_z z), 0] \quad (\text{0}), \quad (12)$$

$$\mathbf{E}_1 = [0, E_{11} \exp(-\kappa_1 z) + E_{12} \exp(\kappa_1 z), 0] \quad (\text{I}), \quad (13)$$

$$\mathbf{E}_{2j} = [0, E_{2j}^1 \exp(-K_{2j} z) + E_{2j}^2 \exp(K_{2j} z), 0] \quad (\text{II}), \quad (14)$$

$$\mathbf{E}_3 = [0, E_3 \exp(\kappa_3 z), 0] \quad (\text{III}). \quad (15)$$

The 0, I, II, and III of (12)–(15) refer to the media of Fig. 7 and in (14) $j = 1, 2$.

We calculate the ATR reflectivity by an extension of the standard matrix method applied by El-Gohary *et al.*⁵³ Applying the electromagnetic and additional boundary conditions to the \mathbf{E} , \mathbf{H} , and \mathbf{u} fields we find

$$S_1 |\mathbf{E}\rangle = S_2 |\mathbf{E}_1\rangle, \quad (16)$$

$$S_3 |\mathbf{E}_{21}\rangle = S_4 |\mathbf{E}_{22}\rangle, \quad (17)$$

$$S_5 |\mathbf{E}_1\rangle = S_6 |\mathbf{E}_{21}\rangle + S_7 |\mathbf{E}_{22}\rangle, \quad (18)$$

$$S_{10} |\mathbf{E}_3\rangle = S_8 |\mathbf{E}_{21}\rangle + S_9 |\mathbf{E}_{22}\rangle. \quad (19)$$

The $|\mathbf{E}_k\rangle$ are two-component column vectors whose elements are the electric field amplitudes in a particular medium and the S_i are 2×2 coefficient matrices. Details of the S_i are contained in Appendix B. After some manipulation we find that the electric-field amplitudes of medium 0, $|\mathbf{E}\rangle$, are related to those of medium III, by

$$|\mathbf{E}\rangle = \Sigma_1 \Sigma_2 |\mathbf{E}_3\rangle, \quad (20)$$

where

$$\Sigma_1 = S_1^{-1} S_2 S_5^{-1} (S_6 S_3^{-1} S_4 + S_7), \quad (21)$$

$$\Sigma_2 = (S_8 S_3^{-1} S_4 + S_9)^{-1} S_{10}. \quad (22)$$

Both $|\mathbf{E}\rangle$ and $|\mathbf{E}_3\rangle$ are of the form $(E_d, E_u)^T$. Here, E_d is the amplitude of the downward ($-z$ direction) traveling wave and E_u is the amplitude of the upward ($+z$ direction) traveling wave. In medium 0 we assume both incident and reflected waves thus $|\mathbf{E}\rangle = (E_i, E_r)^T$. In medium III there is only an evanescent or transmitted field, hence $|\mathbf{E}_3\rangle = (E_t, 0)^T$. The amplitude reflection coefficient, r , $r = E_r / E_i$, is therefore given by (20) to be

$$r(\theta, \omega) = (\Sigma_1 \Sigma_2)_{21} / (\Sigma_1 \Sigma_2)_{11}, \quad (23)$$

and the reflection coefficient is $r^* r = |r|^2$. As mentioned earlier, we keep θ constant and scan the frequency.

The calculated ATR spectrum corresponding to Fig. 3, the dispersion curve for GaAs on NaF in s polarization, is shown in Fig. 8(b), with the zone-center part of Fig. 3 expanded and rotated for comparison in Fig. 8(a). It is seen that there is indeed an ATR dip corresponding to each mode; the coupling strength depends on the mode parity and decreases with the order of the mode.

In p polarization there is the additional longitudinal excitation in medium II, $-a < z < 0$, as well as the two transverse excitations. We take the fields in the form

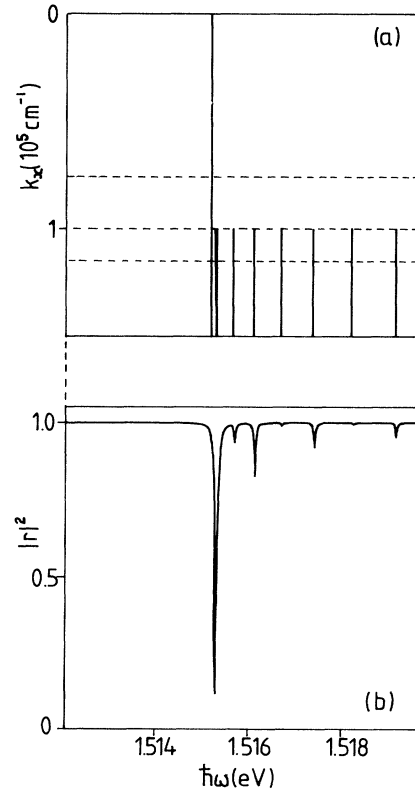


FIG. 8. ATR in s polarization with ABC $\mathbf{u} = \mathbf{0}$ for a $0.1\text{-}\mu\text{m}$ GaAs film on a NaF substrate, corresponding to the dispersion curves of Fig. 3. (a) Zone-center part of dispersion curve, for comparison purposes; (b) calculated ATR spectrum.

$$\mathbf{E}_0 = (k_z, 0, k_x) E_i \exp(-ik_z z) + (-k_z, 0, k_x) E_r \exp(ik_z z) \quad (0), \quad (24)$$

$$\mathbf{E}_1 = (\kappa_1, 0, ik_x) E_{11} \exp(\kappa_1 z) + (-\kappa_1, 0, ik_x) E_{12} \exp(\kappa_1 z) \quad (I), \quad (25)$$

$$\mathbf{E}_{2j} = (K_{2j}, 0, ik_x) E_{2j}^1 \exp(K_{2j} z) + (K_{2j}, 0, ik_x) E_{2j}^2 \exp(K_{2j} z) \quad (II), \quad (26)$$

$$\mathbf{E}_{2L} = (ik_x, 0, K_{2L}) E_{2L}^1 \exp(-K_{2L} z) + (ik_x, 0, -K_{2L}) E_{2L}^2 \exp(K_{2L} z) \quad (II), \quad (27)$$

$$\mathbf{E}_3 = (-\kappa_3, 0, ik_x) E_3 \exp(\kappa_3 z) \quad (III). \quad (28)$$

The 0, I, II, and III of (24) to (28) refer to the media of Fig. 7 and in (26) $j=1,2$.

Applying the boundary conditions to the \mathbf{E} , \mathbf{D} , and \mathbf{u} fields we find

$$P_1 |\mathbf{E}\rangle = P_2 |\mathbf{E}_2\rangle, \quad (29)$$

$$P_3 |\mathbf{E}_1\rangle = P_4 |\mathbf{E}_{21}\rangle + P_5 |\mathbf{E}_{22}\rangle + P_6 |\mathbf{E}_{2L}\rangle, \quad (30)$$

$$P_9 |\mathbf{E}_{2L}\rangle = P_7 |\mathbf{E}_{21}\rangle + P_8 |\mathbf{E}_{22}\rangle, \quad (31)$$

$$P_{12} |\mathbf{E}_{2L}\rangle = P_{10} |\mathbf{E}_{21}\rangle + P_{11} |\mathbf{E}_{22}\rangle, \quad (32)$$

$$P_{16} |\mathbf{E}_3\rangle = P_{13} |\mathbf{E}_{21}\rangle + P_{14} |\mathbf{E}_{22}\rangle + P_{15} |\mathbf{E}_{2L}\rangle. \quad (33)$$

The $|\mathbf{E}_k\rangle$ and P_i are contained in Appendix C.

The electric-field amplitudes of medium 0, $|\mathbf{E}\rangle$ are related to those of medium III, $|\mathbf{E}_3\rangle$, by

$$|\mathbf{E}\rangle = \Pi_1 \Pi_2 |\mathbf{E}_3\rangle, \quad (34)$$

where

$$\Pi_1 = P_1^{-1} P_2 P_3^{-1} [P_4 \Pi + P_5 + P_6 P_9^{-1} (P_7 \Pi + P_8)], \quad (35)$$

$$\Pi_2 = [P_{13} \Pi + P_{14} + P_{15} P_9^{-1} (P_7 \Pi + P_8)]^{-1} P_{16}, \quad (36)$$

$$\Pi = [P_9^{-1} P_7 - P_{12}^{-1} P_{10}]^{-1} [P_{12}^{-1} P_{11} - P_9^{-1} P_8]. \quad (37)$$

As in s polarization, $|\mathbf{E}\rangle$ and $|\mathbf{E}_3\rangle$ have the form $(E_d, E_u)^T$, where E_d is the amplitude of the downward ($-z$ direction) traveling wave and E_u is the amplitude of the upward ($+z$ direction) traveling wave. Hence $|\mathbf{E}\rangle = (E_i, E_r)^T$ has both incident and reflected waves, but there is no upward traveling mode in medium III and so $|\mathbf{E}_3\rangle = (E_3, 0)^T$. The amplitude reflection coefficient is $r = E_r/E_i$, and is therefore given by (34) to be

$$r(\theta, \omega) = (\Pi_1 \Pi_2)_{21} / (\Pi_1 \Pi_2)_{11}. \quad (38)$$

The amplitude reflection coefficient is thus $r^* r = |r|^2$. We again take θ constant and scan frequency ω .

The calculated ATR spectrum corresponding to Fig. 6, the dispersion curve for GaAs on NaF in p polarization, is shown in Fig. 9(b), with the zone-center part of Fig. 6

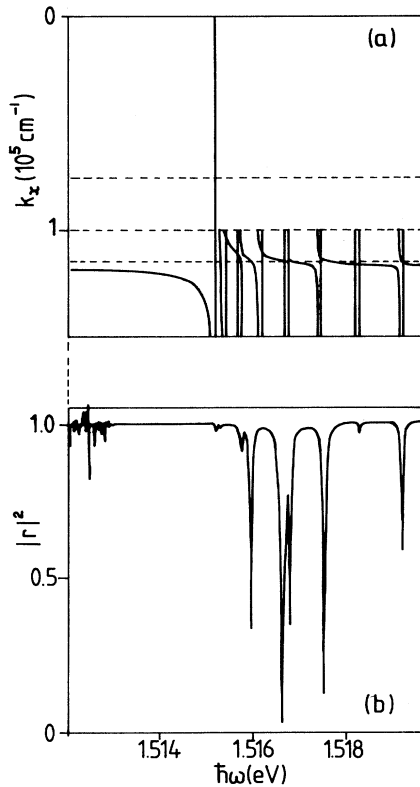


FIG. 9. ATR in p polarization with ABC $\mathbf{u}=\mathbf{0}$ for a $0.1\text{-}\mu\text{m}$ GaAs film on a NaF substrate, corresponding to the dispersion curves of Fig. 6. (a) Zone center of dispersion curve; (b) calculated ATR spectrum.

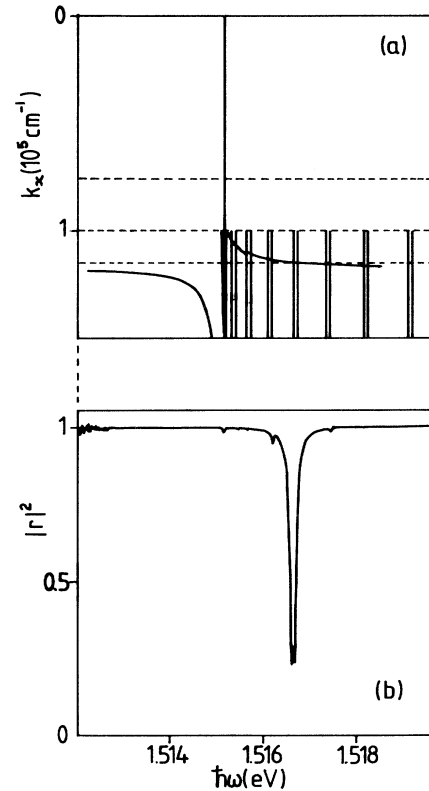


FIG. 10. ATR in p polarization: same as Fig. 9, but with boundary condition $\partial \mathbf{u} / \partial z = 0$.

expanded and rotated for comparison in Fig. 9(a). As for s polarization, Fig. 8, there is indeed a reflectivity dip corresponding to each branch of the dispersion curve. The more complicated mode structure in p polarization is reflected in a more complicated ATR spectrum.

We have also calculated ATR spectra for the alternative boundary condition $\partial u/\partial z=0$. Full details are given elsewhere,⁴⁷ and an example is shown in Fig. 10. The differences between Figs. 9 and 10 are characteristic; in general the coupling to the modes is markedly weaker for the second boundary condition.

V. CONCLUSIONS

We have presented the analytic expressions and some numerical illustrations for both s - and p -polarized exciton polaritons in thin films. Since it is assumed that the excitons have a 3D character, the results are applicable to films of thickness $a \gg a_B$, and within the dead-layer model the thickness appearing in our expressions is to be regarded as an effective thickness $a - 2a_B$. The results should also apply to wide QW's where $a \gg a_B$. In fact, qualitative arguments with the same physical content as our analysis have been applied to experimental results on luminescence and normal-incidence reflectivity on QW systems (Tuffigo *et al.*²³ Shultheis and Ploog,²⁴ and Kusano *et al.*⁴⁶). In the work of Tuffigo *et al.* on luminescence spectra of CdTe QW's, the main free-exciton luminescence peak has satellites in the high-frequency side which are attributed to exciton polaritons with quantized values of k_z . The positions of these satellites are in fact the $k_x=0$ points of our dispersion curves. Very recently, Chen *et al.*⁵⁴ have observed a large number of oscillations in the normal-incidence reflectance of a high-quality GaAs quantum well. Their interpretation of the spectra employs exactly the $k_x=0$ version of the model used here. A calculation allowing for nonzero k_x , such as we have presented, gives a more complete picture of the exciton-polariton spectrum.

Normal-incidence reflectivity measurements probe the s -polarized modes with $k_x=0$. Much more information is available in principle, from ATR measurements, which can probe both s and p polarization over a range of k_x values. We therefore calculated ATR spectra as well as dispersion curves for a film on a substrate. In Figs. 3 and 6 we see that the limiting mechanical-like exciton polaritons ($\partial\omega/\partial k_x \approx 0$) and the limiting photon-polaritonlike ($\partial\omega/\partial k_x \gg 0$) exciton polaritons produce an array of mode anticrossings and mode interactions. We see this most clearly in s polarization, where modes of one "symmetry" interact only with modes of the same kind of symmetry. In p polarization we see the same effect, but it occurs very much closer to the zone center, in fact along the limiting p polarized photon-polariton dispersion curve. In p polarization we also note the complications due to the longitudinal modes in the form of coupling between all the modes. In the ATR figures we see that the deepest resonances are caused by those modes which are in a photon-polaritonlike state ($\partial\omega/\partial k_x \gg 0$) with all the other more mechanical-like exciton polaritons ($\partial\omega/\partial k_x \approx 0$) producing only weak resonances. The difference between the two ABC's $\mathbf{u}=0$ and $\partial\mathbf{u}/\partial z=0$ in

the numerical analysis for the dispersion curves and in the ATR calculations is pronounced. First, the mode anticrossings occur on a much finer scale for the second ABC than the first. Second, the higher modes are shifted down in energy; this explains a splitting of the resonance for s polarization for the second ABC, since a mode has been shifted down in energy to coincide with a photon-polaritonlike mode. Third, the coupling in the ATR experiment is generally much weaker for the second ABC than the first.

In view of this analysis we suggest that the corresponding experiment would be a useful tool in determining the actual ABC for the thin-film exciton-polariton problem. It may be, however, that this approach is limited to films of thickness $a \approx 10a_B$, where a_B is the excitonic Bohr radius, since for thicker films the energy separation of modes rapidly decreases so that the individual resonances of the modes would merge. It would then be difficult to locate precisely the ABC-dependent features. Such an effect is in fact found by Kusano *et al.*⁴⁶ Their photoluminescence spectra contain sharp exciton-polariton peaks for films of thickness 99 and 201 nm, as discussed earlier, but they see no such peaks for a film of thickness 520 nm.

For thinner films, where the 2D character of the excitons becomes important, a microscopic analysis is required. A major contribution is made by Andreani and Bassani,⁵⁵ who give a derivation of the nonlocal dielectric kernel $\epsilon(z, z', k_x)$ in an integral formulation, and apply the result to a derivation of the exciton-polariton dispersion curves in films of thickness 10 nm or less.

ACKNOWLEDGMENTS

R.N.P. thanks the Science and Engineering Research Council (SERC) for partial support, and GEC for further financial support.

APPENDIX A: DISPERSION EQUATION

For the symmetric geometry in s polarization the dispersion equation is

$$M^2 \begin{vmatrix} X_0 \mathcal{C}_1 + X_1 \mathcal{S}_1 & X_0 \mathcal{C}_2 + X_2 \mathcal{S}_2 \\ d_2 \mathcal{C}_1 & d_1 \mathcal{C}_2 \end{vmatrix} \\ \times \begin{vmatrix} d_1 \mathcal{S}_2 & d_2 \mathcal{S}_1 \\ X_0 \mathcal{S}_2 + X_2 \mathcal{C}_2 & X_0 \mathcal{S}_1 + X_1 \mathcal{C}_1 \end{vmatrix} \\ + N^2 \begin{vmatrix} X_0 \mathcal{C}_2 + X_2 \mathcal{S}_2 & X_0 \mathcal{C}_1 + X_1 \mathcal{S}_1 \\ d_1 X_2 \mathcal{S}_2 & d_2 X_1 \end{vmatrix} \\ \times \begin{vmatrix} d_1 X_2 \mathcal{C}_2 & d_2 X_1 \mathcal{C}_1 \\ X_0 \mathcal{S}_2 + X_2 \mathcal{C}_2 & X_0 \mathcal{S}_1 + X_1 \mathcal{C}_1 \end{vmatrix} = 0, \quad (\text{A1})$$

where

$$\mathcal{C}_j = (f_j + g_j)/2, \quad (\text{A2})$$

$$\mathcal{S}_j = (f_j - g_j)/2, \quad (\text{A3})$$

$$f_j = \exp(K_j a/2), \quad (\text{A4})$$

$$g_j = \exp(-K_j a/2), \quad (\text{A5})$$

$$d_j = 1 - \frac{\omega^2}{\omega_e^2} + \frac{D}{\omega_e^2} (k_x^2 - K_j^2), \quad (\text{A6})$$

$$X_0 = \kappa_1 c / \omega_e, \quad (\text{A7})$$

$$X_j = K_j c / \omega_e. \quad (\text{A8})$$

For the symmetric geometry in p polarization the disper-

sion equation is

$$\begin{vmatrix} \underline{A}_1 & \underline{A}_2 \\ \underline{A}_3 & \underline{A}_4 \end{vmatrix} = 0, \quad (\text{A9})$$

where

$$\underline{A}_1 = \begin{pmatrix} (\epsilon \mathcal{S}_1 X_1 + \eta_1 \mathcal{C}_1 X_0) X_2 & (\epsilon \mathcal{S}_2 X_2 + \eta_2 \mathcal{C}_2 X_0) X_1 & \epsilon \mathcal{S}_L X_1 X_2 \\ -\alpha \mathcal{C}_1 N X_1 d_2 & -\alpha \mathcal{C}_2 N X_2 d_1 & N \mathcal{C}_L \epsilon_\infty X_L d_1 d_2 \\ -N \alpha d_1 Q^2 \mathcal{S}_1 X_1 X_2 & -N \alpha d_1 Q^2 \mathcal{S}_2 X_1 X_2 & \epsilon_\infty N \mathcal{S}_L X_1 X_2 X_L^2 d_1 d_2 \end{pmatrix}, \quad (\text{A10})$$

$$\underline{A}_2 = \begin{pmatrix} 0 & 0 & 0 \\ -\mathcal{C}_L \epsilon_\infty M d_1 d_2 & \alpha \mathcal{C}_2 M d_1 & \alpha \mathcal{C}_1 M d_2 \\ -\epsilon_\infty M \mathcal{S}_L X_1 X_2 X_L d_1 d_2 & \alpha M Q^2 \mathcal{S}_2 X_1 d_1 & \alpha M Q^2 \mathcal{S}_1 X_2 d_2 \end{pmatrix}, \quad (\text{A11})$$

$$\underline{A}_3 = \begin{pmatrix} \alpha \mathcal{C}_1 M Q^2 X_2 d_2 & \alpha \mathcal{C}_2 M Q^2 X_1 d_1 & -\mathcal{C}_L \epsilon_\infty M X_1 X_2 X_L d_1 d_2 \\ \alpha M \mathcal{S}_1 d_2 & \alpha M \mathcal{S}_2 d_1 & -\alpha \epsilon_\infty M \mathcal{S}_L d_1 d_2 \\ 0 & 0 & 0 \end{pmatrix}, \quad (\text{A12})$$

$$\underline{A}_4 = \begin{pmatrix} \mathcal{C}_L \epsilon_\infty N X_1 X_2 X_L^2 d_1 d_2 & -\alpha \mathcal{C}_2 N Q^2 X_1 X_2 d_1 & -\mathcal{C}_1 Q^2 X_1 X_2 d_2 \\ \epsilon_\infty N \alpha \mathcal{S}_L X_L d_1 d_2 & -\alpha N \mathcal{S}_2 X_2 d_1 & -\alpha N \mathcal{S}_1 X_1 d_2 \\ \mathcal{C}_L \epsilon X_1 X_2 & (\eta_2 \mathcal{S}_2 X_0 + \mathcal{C}_2 \epsilon X_2) X_1 & (\eta_1 \mathcal{S}_1 X_0 + \mathcal{C}_1 \epsilon X_1) X_2 \end{pmatrix}. \quad (\text{A13})$$

Here \mathcal{C}_L , \mathcal{S}_L , and X_L are defined by analogy with (A2), (A3), and (A8). The other quantities are

$$\alpha = S / \omega_e^2 \quad (\text{A14})$$

and

$$\eta_j = \epsilon_\infty + S / [\omega_e^2 - \omega^2 + D(k_x^2 - K_j^2)]. \quad (\text{A15})$$

APPENDIX B: s -POLARIZATION ATR TRANSFER MATRICES

The coefficient matrices \underline{S} are

$$\underline{S}_1 = \begin{pmatrix} g & f \\ ik_z g & -ik_z f \end{pmatrix}, \quad \underline{S}_2 = \begin{pmatrix} g_1 & f_1 \\ \kappa_1 g_1 & -\kappa_1 f_1 \end{pmatrix},$$

$$\underline{S}_3 = \begin{pmatrix} \alpha_1 \lambda_1^- & \alpha_1 \lambda_1^+ \\ \alpha_1 \lambda_1^- f_{21} & \alpha_1 \lambda_1^+ g_{21} \end{pmatrix},$$

$$\underline{S}_4 = \begin{pmatrix} -\alpha_2 \lambda_2^- & -\alpha_2 \lambda_2^+ \\ -\alpha_2 \lambda_2^- f_{22} & -\alpha_2 \lambda_2^+ g_{22} \end{pmatrix},$$

$$\underline{S}_5 = \begin{pmatrix} 1 & 1 \\ \kappa_1 & -\kappa_1 \end{pmatrix}, \quad \underline{S}_6 = \begin{pmatrix} 1 & 1 \\ K_{21} & -K_{21} \end{pmatrix},$$

$$\underline{S}_7 = \begin{pmatrix} 1 & 1 \\ K_{22} & -K_{22} \end{pmatrix}, \quad \underline{S}_8 = \begin{pmatrix} f_{21} & g_{21} \\ K_{21} f_{21} & -K_{21} g_{21} \end{pmatrix},$$

$$\underline{S}_9 = \begin{pmatrix} f_{22} & g_{22} \\ K_{22} f_{22} & -K_{22} g_{22} \end{pmatrix},$$

$$\underline{S}_{10} = \begin{pmatrix} g_3 & 0 \\ -\kappa_3 g_3 & 0 \end{pmatrix}.$$

The symbols not previously defined are

$$\lambda_j^\pm = M \pm N K_{2j}, \quad f_{2j} = \exp(K_{2j} a), \\ g_{2j} = \exp(-K_{2j} a), \quad \alpha_j = (c^2 / \omega^2) (k_x^2 - K_{2j}^2) - \epsilon_\infty.$$

APPENDIX C: p -POLARIZATION ATR TRANSFER MATRICES

The coefficient matrices \underline{P}_i are

$$\underline{P}_1 = \begin{pmatrix} k_x g & -k_z f \\ \epsilon g & \epsilon f \end{pmatrix}, \quad \underline{P}_2 = \begin{pmatrix} \kappa_1 g_1 & -\kappa_1 f_1 \\ i \epsilon_1 g_1 & i \epsilon_1 f_1 \end{pmatrix},$$

$$\underline{P}_3 = \begin{pmatrix} \kappa_1 & -\kappa_1 \\ \epsilon_1 & \epsilon_1 \end{pmatrix}, \quad \underline{P}_4 = \begin{pmatrix} K_{21} & -K_{21} \\ \eta_1 & \eta_1 \end{pmatrix},$$

$$\underline{P}_5 = \begin{pmatrix} K_{22} & -K_{22} \\ \eta_2 & \eta_2 \end{pmatrix}, \quad \underline{P}_6 = \begin{pmatrix} -ik_x & ik_x \\ 0 & 0 \end{pmatrix},$$

$$\underline{P}_7 = \begin{pmatrix} K_{21} \alpha_1 \lambda_1^- & -K_{21} \alpha_1 \lambda_1^+ \\ ik_x \alpha_1 \lambda_1^- & ik_x \alpha_1 \lambda_1^+ \end{pmatrix},$$

$$\underline{P}_8 = \begin{pmatrix} K_{22} \alpha_2 \lambda_2^- & -K_{22} \alpha_2 \lambda_2^+ \\ ik_x \alpha_2 \lambda_2^- & ik_x \alpha_2 \lambda_2^+ \end{pmatrix},$$

$$\underline{P}_9 = \begin{pmatrix} ik_x \epsilon_\infty \lambda_L^- & \lambda_L^+ \\ K_L \epsilon_\infty \lambda_L^- & K_L \epsilon_\infty \lambda_L^+ \end{pmatrix},$$

$$\underline{P}_{10} = \begin{pmatrix} K_{21} \alpha_1 \lambda_1^- f_{21} & -K_{21} \alpha_1 \lambda_1^+ g_{21} \\ ik_x \alpha_1 \lambda_1^- f_{21} & ik_x \alpha_1 \lambda_1^+ g_{21} \end{pmatrix},$$

$$\underline{P}_{11} = \begin{pmatrix} K_{22} \alpha_2 \lambda_2^- f_{22} & -K_{22} \alpha_2 \lambda_2^+ g_{22} \\ ik_x \alpha_2 \lambda_2^- f_{22} & ik_x \alpha_2 \lambda_2^+ g_{22} \end{pmatrix},$$

$$\underline{P}_{12} = \begin{bmatrix} -k_x \epsilon_\infty \lambda_L^- f_L & ik_x \epsilon_\infty \lambda_L^+ g_L \\ K_L \epsilon_\infty \lambda_L^- f_L & K_L \epsilon_\infty \lambda_L^+ g_L \end{bmatrix},$$

$$\underline{P}_{13} = \begin{bmatrix} K_{21} f_{21} & -K_{21} g_{21} \\ \eta_1 f_{21} & \eta_1 g_{21} \end{bmatrix},$$

$$\underline{P}_{14} = \begin{bmatrix} K_{22} f_{22} & -K_{22} g_{22} \\ \eta_2 f_{22} & \eta_2 g_{22} \end{bmatrix},$$

$$\underline{P}_{15} = \begin{bmatrix} -ik_x f_L & k_x g_L \\ 0 & 0 \end{bmatrix},$$

$$\underline{P}_{16} = \begin{bmatrix} -\kappa_3 g_3 & 0 \\ \epsilon_3 g_3 & 0 \end{bmatrix}.$$

The previously undefined symbols are

$$f_L = \exp(K_L a / 2), \quad g_L = \exp(-K_L a / 2).$$

- *Present address: Research Institute of Electrical Communication, Tohoku University, Sendai 980, Japan.
- ¹S. I. Pekar, Zh. Eksp. Teor. Fiz. **33**, 1022 (1957) [Sov. Phys. JETP **6**, 785 (1957)].
- ²S. I. Pekar, Fiz. Tverd. Tela (Leningrad) **4**, 1301 (1962) [Sov. Phys. Solid State **4**, 953 (1962)].
- ³J. J. Hopfield, Phys. Rev. **112**, 1555 (1958).
- ⁴J. J. Hopfield and D. G. Thomas, J. Phys. Chem. Solids **12**, 276 (1960).
- ⁵J. J. Hopfield and D. G. Thomas, Phys. Rev. **132**, 563 (1963).
- ⁶A. A. Maradudin and D. L. Mills, Phys. Rev. **B 7**, 2787 (1973).
- ⁷R. Dingle, Festkörperprobleme **XV**, 21 (1975).
- ⁸L. Greene, K. Bajaj, and D. E. Phelps, Phys. Rev. **B 29**, 1087 (1984).
- ⁹V. C. Y. So, J. E. Sipe, M. Fukui, and G. I. Stegeman, J. Phys. **C 14**, 4487 (1981).
- ¹⁰V. C. Y. So, J. E. Sipe, M. Fukui, and G. I. Stegeman, J. Phys. **C 14**, 4505 (1981).
- ¹¹P. Halevi, J. Phys. **C 16**, 3713 (1982).
- ¹²P. Halevi in *Excitons in Confined Systems*, edited by R. Del Sole, A. D'Andrea, and A. Lapicciarella, Springer Proceedings in Physics Vol. 25 (Springer Verlag, Berlin, 1988), p. 2.
- ¹³P. Halevi, G. Hernandez-Cocoletzi, and F. Ramos, *Excitons in Confined Systems* (Ref. 12), p. 35.
- ¹⁴J. S. Nkoma, J. Phys. **C 16**, 3713 (1983).
- ¹⁵M. Matsushita, J. Wickstead, and H. Z. Cummins, Phys. Rev. **B 29**, 3362 (1984).
- ¹⁶R. Del Sole and A. D'Andrea, *Excitons in Confined Systems* (Ref. 12), p. 14.
- ¹⁷I. Basilev, *Excitons in Confined Systems* (Ref. 12), p. 82.
- ¹⁸C. S. Ting, M. J. Frankel, and J. L. Birman, Solid State Commun. **17**, 1285 (1975).
- ¹⁹E. L. Ivchenko and V. A. Kosobukhin, Fiz. Tekh. Poluprovodn. **22**, 24 (1988) [Sov. Phys. Semicond. **22**, 15 (1988)].
- ²⁰G. S. Agarwal, D. N. Pattanayk, and E. Wolf, Phys. Rev. Lett. **27**, 1022 (1971).
- ²¹P. G. de Gennes, *Superconductivity of Metals and Alloys* (Benjamin, New York, 1966).
- ²²D. R. Tilley, J. Phys. **C 13**, 781 (1980).
- ²³H. Tuffigo, R. T. Cox, N. Magnea, Y. Merle D'Aubigne, and A. Million, Phys. Rev. **B 37**, 4310 (1988).
- ²⁴L. Schultheis and K. Ploog, Phys. Rev. **B 30**, 1090 (1984).
- ²⁵V. A. Kiselev, R. Z. Razbirin, I. N. Ural'tsev, and V. P. Kochereshko, Fiz. Tverd. Tela **17**, 640 (1975) [Sov. Phys. Solid State **17**, 418 (1975)].
- ²⁶M. Born and K. Huang, *Dynamical Theory of Crystal Lattices* (Clarendon, Oxford, 1954).
- ²⁷R. S. Knox, *Theory of Excitons* (Academic, New York, 1963), Chap. 2.
- ²⁸*Polarons and Excitons*, Scottish Universities Summer School, St. Andrews, Scotland, edited by C. G. Kuper and G. D. Whitfield (Oliver and Boyd, Edinburgh, 1962).
- ²⁹W. A. Washington, A. Z. Genack, H. Z. Cummins, R. H. Bruce, R. A. Compaan, and R. A. Forman, Phys. Rev. **B 15**, 2145 (1977).
- ³⁰W. Brenig, R. Zeyher, and J. L. Birman, Phys. Rev. **B 6**, 4617 (1972).
- ³¹C. Weisbuch and R. G. Ulbrich, Phys. Rev. Lett. **38**, 865 (1977).
- ³²C. Hermann and P. Y. Yu, Solid State Commun. **28**, 313 (1978).
- ³³B. Sermage and G. Fishman, Phys. Rev. Lett. **43**, 1043 (1979).
- ³⁴A. Otto, Z. Phys. **216**, 298 (1968).
- ³⁵J. Lagois and B. Fischer in *Surface-Polaritons*, edited by V. M. Agranovich and D. L. Mills (North-Holland, Amsterdam, 1982).
- ³⁶J. Lagois and B. Fischer, Phys. Rev. **B 36**, 680 (1976).
- ³⁷I. Hirabayashi, K. Tokura, and T. Koda, J. Phys. Soc. Jpn. **51**, 2934 (1982).
- ³⁸Y. Tokuru, I. Hirabayashi, and T. Koda, J. Phys. Soc. Jpn. **50**, 145 (1981).
- ³⁹P. R. Rimbey, Phys. Rev. **B 15**, 1215 (1977).
- ⁴⁰J. Lagois and B. Fischer, Solid State Commun. **18**, 1519 (1976).
- ⁴¹V. A. Kiselev, B. S. Razbirin, and I. N. Ural'tser, Pis'ma Zh. Eksp. Teor. Fiz. **18**, 504 (1973) [JETP Lett. **18**, 296 (1973)].
- ⁴²V. A. Kiselev, B. S. Razbirin, and I. N. Ural'tser, Phys. Status Solidi **B 72**, 161 (1975).
- ⁴³X. L. Zheng, D. Heinman, B. Lax, and F. A. Chambers, Appl. Phys. Lett. **52**, 287 (1988).
- ⁴⁴F. Yang, J. R. Sambles, and G. W. Bradberry, Phys. Rev. Lett. **64**, 559 (1990).
- ⁴⁵M. Kohl, D. Heitmann, P. Gramlow, and K. Ploog, Phys. Rev. **B 37**, 10927 (1988).
- ⁴⁶J. Kusano, Y. Segawa, M. Mihara, Y. Aoyagi, and S. Namba, Solid State Commun. **72**, 215 (1989).
- ⁴⁷R. N. Philp, Ph.D. thesis, University of Essex, 1989.
- ⁴⁸G. W. C. Kaye and T. H. Laby, *Tables of Physical Constants* (Cambridge University Press, Cambridge, 1976).
- ⁴⁹W. J. Rappel, L. F. Feiner, and M. F. H. Schurmans, *Excitons in Confined Systems* (Ref. 12), p. 63.
- ⁵⁰M. G. Cottam, and D. R. Tilley, *Introduction to Surface and Superlattice Excitations* (Cambridge University Press, Cambridge, 1989).
- ⁵¹F. Abeles, in *Electromagnetic Surface Excitations*, edited by R. F. Wallis and G. I. Stegeman (Springer-Verlag, Berlin 1986), p. 8.
- ⁵²M. Fukui, A. Kamada, and O. Toda, J. Phys. Soc. Jpn. **53**, 1185 (1984).
- ⁵³A. R. El-Gohary, T. J. Parker, N. Raj, D. R. Tilley, P. J. Dobson, D. Hilton, and C. T. B. Foxon, Semicond. Sci. Technol. **4**, 388 (1989).
- ⁵⁴Y. Chen, F. Bossani, J. Massies, C. Depavis, and G. Neu, Europhys. Lett. **41**, 483 (1991).
- ⁵⁵L. C. Andreani and F. Bassani, Phys. Rev. **B 41**, 7536 (1990).